

Magnitude-Period Scaling Relations for Japan and the Pacific Northwest: Implications for Earthquake Early Warning

by Andrew B. Lockman and Richard M. Allen

Abstract Scaling relations between the predominant period of P -wave arrivals and earthquake magnitude are explored using datasets from the Pacific Northwest and Japan, and compared with previous observations in southern California (Allen and Kanamori, 2003). We find the same scaling for events in all three geologically diverse regions. The sensitivity of the predominant period observation to magnitude can be optimized using various frequency bands for different magnitude ranges and in different regions. The ability to estimate the magnitude using the first few seconds of the P wave offers a methodology for earthquake early warning. The accuracy of magnitude estimates increases with the number of stations reporting predominant period observations. The most significant improvements in the magnitude estimate occur when the number of reporting stations increased from one to four. As in southern California, we find that the average absolute magnitude error is ~ 0.5 magnitude units when the closest four stations to the epicenter are used.

Introduction

Most seismic-hazard mitigation efforts focus on long-term earthquake forecasting using probabilistic ground-shaking hazard maps (Frankel *et al.*, 1996) and rapid post-event assessments to determine which areas experienced the most severe shaking and require immediate disaster relief (Wald *et al.*, 1999). Short-term seismic mitigation involves early warning systems (EWSs), which issue an alert while the earthquake is occurring. The concept of EWS was proposed in 1868 by J. D. Cooper, in the *San Francisco Daily Evening Bulletin*, who noticed that earthquake waves travel much slower than electronic communication systems, and proposed an automated system of sensors that would trigger on large seismic waves and sound a warning bell in San Francisco before the wave's arrival. Many years passed before Cooper's idea was put into practice, but modern EWSs use the concept he described to quickly estimate earthquake magnitude and issue a warning to areas at risk of severe shaking several seconds before ground shaking begins.

EWSs are currently operational in Mexico, Taiwan, Turkey, and Japan. Mexico City employs a Seismic Alert System (SAS) that operates with a method known as front detection. The SAS measures peak ground motion near the Guerrero Gap subduction zone to estimate earthquake magnitude, and transmits this information to the population in Mexico City 300 km away, giving 60 sec or more warning (Espinosa-Aranda *et al.*, 1995). The Central Weather Bureau in Taiwan also uses front detection to locate and determine the magnitude of an earthquake. Their method requires an average of 22 sec for magnitude determination and gives

warning to populations greater than 75 km away (Wu *et al.*, 1998; Wu and Teng, 2002). Development of a method using the P -wave arrival is now underway to increase warning times (Wu and Kanamori, 2005). Turkey recently implemented their warning system, which triggers when the amplitude of ground motion exceeds some threshold (Erdik *et al.*, 2003; Boese *et al.*, 2004). In the mid-1960s, Japan Railways developed a front detection system to help prevent high-speed trains from crossing track damaged during an earthquake (Nakamura and Tucker, 1988), and since then has developed more sophisticated methods that use P -wave arrivals to determine the event magnitude and location (Nakamura, 1988, 2004). The Japan Meteorological Agency has been testing an EWS with broader application since February 2004 (Odaka *et al.*, 2003; Kamigaichi, 2004; Horiuchi *et al.*, 2005). In August 2006 they widened the testing to 41 institutions, including railway companies, construction firms, factories, and hospitals. As the public becomes more familiar with the system they plan to make the information more widely available.

The P -wave detection approach gives more warning time than systems that must wait for peak ground-motion observations, but accurately describing the relation between the P wave and magnitude has proved difficult. Grecksch and Kumpel (1997) used a large dataset containing earthquakes from North and Central America to demonstrate that the first second of the P wave can be used to estimate the magnitude within 0.5 magnitude units by using parameters derived from strong motion sensors including the frequency

content, peak acceleration, peak spectral amplitude, and the rise time when data are gathered from more than eight seismic stations.

Previous studies of earthquakes in southern California show a scaling relation between the predominant period of the *P* wave (a spectrally weighted measure of a signal's frequency content) and event magnitude (Allen and Kanamori, 2003; Allen, 2004; Lockman and Allen, 2005). The scaling relation shows that small earthquakes radiate high-frequency energy, whereas larger earthquakes emit lower-frequency energy. Implicit in this relation is that the frequency content of the *P* wave carries information pertaining to the overall size of the fault rupture, and thus earthquake magnitude. Here we focus on the empirical observation and how it can be used for the purpose of earthquake early warning; the implications of the scaling relation for earthquake rupture are discussed by Olson and Allen (2005).

Rydelek and Horiuchi (2006) used the same methodology described here to look for a scaling relation in a dataset from Japan but were unable to identify a relation similar to the one observed in southern California. This may be due, at least in part, to the limited magnitude range that they used (Olson and Allen, 2006). Here we make use of a larger dataset from Japan and find a scaling relation between predominant period and magnitude just as in southern California.

Wolfe (2006) has also explored the properties of the predominant period observation identifying limitations to the methodology that introduce errors into the observations. Whether these are significant compared with those introduced by station site effects (Lockman and Allen, 2005) remains to be determined. Removing some of these nonideal

properties of the predominant period measurement, Simons *et al.* (2006) develop an alternative approach to measure predominant period using wavelet multiscale analysis. They apply their method to data from southern California and obtain a scaling relation very similar to that obtained by Allen and Kanamori (2003). Here we apply the same approach used in southern California by Allen and Kanamori (2003), and on a global dataset by Olson and Allen (2005), and we apply it to earthquake data from Japan and the Pacific Northwest with as wide a magnitude range as possible.

By analyzing earthquake data from Japan and the Pacific Northwest we are able to increase the magnitude range of events studied, in particular, the number of large-magnitude events, and also investigate whether there are differences in the scaling relations in various geological settings. The present study uses earthquakes with magnitudes ranging from 3.5 up to the largest magnitudes for which data were available from the Pacific Northwest and Japan. Our results indicate an scaling relation exists equivalent to that observed in southern California, and the accuracy of magnitude estimates based on predominant period can be improved with the application of regionally defined low-pass filters.

Datasets

Two datasets were created using earthquakes that occurred in the Pacific Northwest and Japan and were recorded on broadband velocity instruments within 150 km of the epicenter (Fig. 1). All waveforms recorded within 150 km of each event epicenter containing a clear *P*-wave arrival without clipping during the first 5 sec of the signal were used

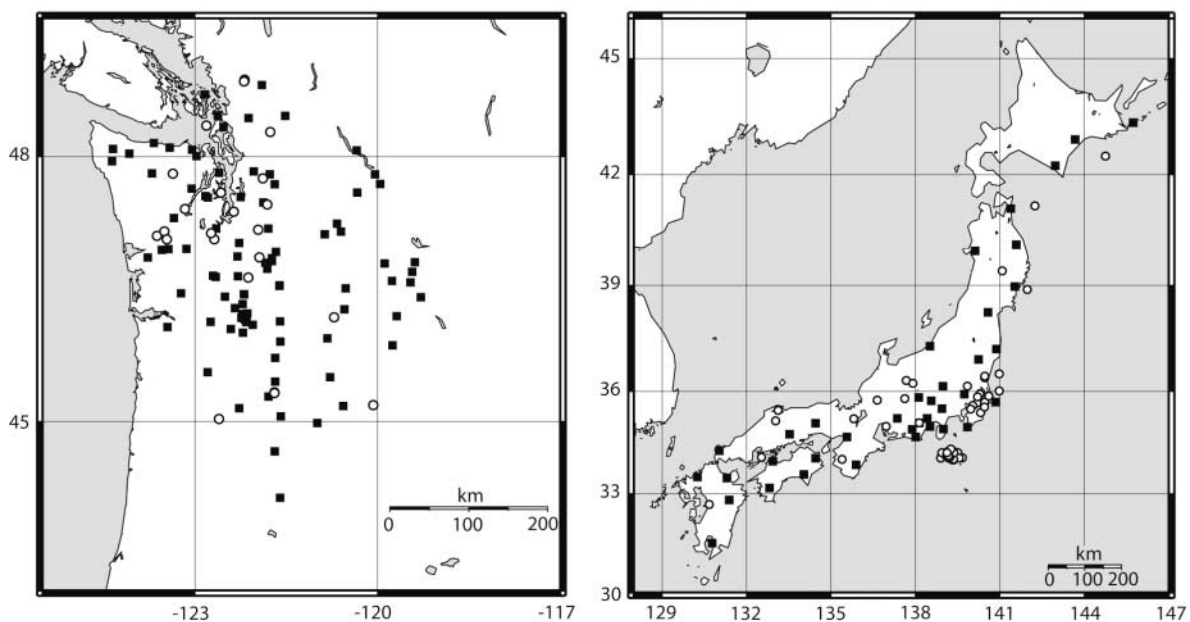


Figure 1. Maps showing the locations of events and stations providing waveform data from the Pacific Northwest (left) and Japan (right). Epicentral locations of earthquakes are shown with circles, and the locations of broadband velocity instruments that recorded the events are shown with squares.

in the study. The Pacific Northwest dataset contains 25 earthquakes ranging in magnitude from 3.5 to 6.8 that occurred between 1989 and 2001 and were recorded by the Pacific Northwest Seismograph Network (Ludwin *et al.*, 1994) (Table 1). This dataset includes randomly selected events with magnitudes between 3.5 and 4.5 and every event greater than 4.5. The Japan dataset contains 62 earthquakes recorded by the Broadband Seismic Network Laboratory of the National Research Institute for Earth Science and Disaster Prevention in Japan (Okada *et al.*, 2004) between 1998 and 2002, and includes 48 randomly selected events of magnitude 3.8–5.7 and every event greater than 5.7 (Table 2).

Predominant Period Observations

The ability to estimate the magnitude of an earthquake with the P wave is based on the analysis of its predominant period (T^p), a measure of the frequency content of the seismic signal. T^p is continuously calculated in a causal fashion from the vertical component of velocity waveforms using the approach of Allen and Kanamori (2003), based on the method described by Nakamura (1988), using the following relation:

$$T_i^p = 2\pi\sqrt{X_i/D_i}, \quad (1)$$

where

$$X_i = \alpha X_{i-1} + x_i^2 \quad (2)$$

$$D_i = \alpha D_{i-1} + (dx/dt)_i^2 \quad (3)$$

and T_i^p is the predominant period for sample i , x_i is the recorded ground velocity, X_i is the smoothed ground velocity squared, D_i is the smoothed velocity derivative squared, and α is a smoothing constant set equal to 0.999.

To understand the origin of the measurement consider the case where $\alpha = 1$. Then equation (2) becomes

$$X_i = X_{i-1} + x_i^2 \quad (4)$$

which is an integration of x^2 . In this case, and for a continuous time series, equation (1) becomes

$$\tau = 2\pi \sqrt{\frac{\int_0^{t_0} x^2(t) dt}{\int_0^{t_0} \dot{x}^2(t) dt}}, \quad (5)$$

where 0 is the arbitrary starting time and t_0 is the time at which τ can be calculated. In equation (5) we use τ instead of T_i^p because equation (5) is for the continuous case; T_i^p used in equation (1) is the discrete case. Using Parseval's equality, the ratio

Table 1
Event Source Parameters for Earthquakes in the Pacific Northwest That Were Used in This Study

Date	Time	Magnitude	Latitude	Longitude	Depth (km)	No. of Waveforms Collected for Event
3/5/1989	06.42.00.66	4.6	47.81	-123.36	46	2
12/24/1989	08.45.58.90	5.1	46.65	-122.12	18	3
3/8/1990	22.11.09.35	3.6	48.27	-121.76	1	11
4/3/1990	02.18.20.81	4.1	48.84	-122.18	1	6
4/14/1990	06.02.49.53	3.6	48.83	-122.18	3	9
4/14/1990	05.40.07.26	4.2	48.82	-122.19	3	4
10/19/1990	14.13.58.16	3.5	45.34	-121.69	6	22
12/30/1990	02.20.56.99	3.5	47.47	-121.81	17	19
10/25/1991	15.42.06.26	3.8	47.12	-123.62	38	10
3/13/1992	04.12.42.29	3.7	48.34	-122.81	17	9
6/8/1993	00.01.25.25	3.7	45.03	-122.60	20	9
6/15/1994	08.22.19.76	4.0	47.42	-123.16	44	4
9/10/1994	07.43.11.33	4.1	47.19	-121.96	18	4
1/29/1995	03.11.22.67	5.1	47.39	-122.36	17	4
5/20/1995	12.48.48.21	4.2	46.88	-121.94	13	8
5/3/1996	04.04.22.67	5.5	47.76	-121.88	4	3
3/22/1997	06.05.34.97	3.9	45.19	-120.07	1	11
6/23/1997	19.13.27.04	5.0	47.60	-122.57	7	4
10/9/1998	16.43.08.29	4.0	46.20	-120.71	3	23
7/3/1999	00.1.43.54	5.8	47.08	-123.46	40	4
2/28/2001	18.54.32.83	6.8	47.15	-122.73	51	4
6/10/2001	13.19.11.29	5.0	47.17	-123.50	40	2
7/22/2001	15.13.52.60	4.3	47.08	-122.68	50	8
6/29/2002	14.36.04.79	4.5	45.33	-121.69	6	4

Table 2
Event Source Parameters for Earthquakes in Japan That Were Used in This Study

Date	Time	Magnitude	Latitude	Longitude	Depth (km)	No. of Waveforms Collected for Event
8/9/1998	3:45:25.07	3.9	36.32	137.68	10	6
8/24/1998	2:18:34.78	4.1	34.18	139.18	33	3
11/25/1998	1:47:55.68	4.2	35.75	136.65	33	2
11/27/1998	15:22:58.51	4.5	35.60	140.04	66	7
12/22/1998	10:23:12.32	4.4	35.93	140.30	97	6
1/28/1999	1:25:43.31	4.9	36.24	137.92	10	8
3/14/1999	1:34:33.42	4.2	34.28	139.28	33	6
3/14/1999	0:04:44.53	5.1	34.13	139.09	33	5
3/16/1999	7:43:36.93	5.1	35.21	135.82	33	3
3/25/1999	23:31:11.4	5.2	36.40	140.47	82	3
3/27/1999	16:37:05.59	4.8	34.06	138.90	39	7
4/5/1999	6:13.85	3.9	35.80	137.63	33	7
4/25/1999	12:27:05.27	5.3	36.44	140.47	81	3
5/7/1999	12:48:27.06	4.8	35.09	138.14	33	7
7/14/1999	22:56:23.29	5.2	35.85	140.21	83	6
7/22/1999	21:53:47.26	4.9	36.02	140.98	64	2
8/20/1999	20:33:10.88	5.7	34.02	135.40	65	3
9/12/1999	22:56:46.39	5.4	35.49	139.97	64	8
11/29/1999	12:34:02.51	4.6	34.99	136.97	45	7
12/3/1999	18:28:38.13	4.0	35.69	140.47	33	3
12/4/1999	5:06:12.19	5.0	35.87	140.61	95	3
6/3/2000	8:54:49.2	6.2	35.55	140.46	62	5
6/8/2000	0:32:46.5	5.0	32.68	130.68	21	3
6/27/2000	5:25:13.62	4.5	34.10	139.37	10	3
6/28/2000	8:52:19.85	3.8	34.07	139.67	10	2
6/28/2000	14:20:09.97	4.6	34.24	139.39	10	7
6/28/2000	16:15:17.96	5.2	34.01	139.32	10	4
6/28/2000	9:25:47.89	5.3	34.22	139.51	10	5
6/29/2000	4:02:36.92	5.5	34.06	139.56	10	3
6/29/2000	6:30:22.09	5.6	34.03	139.36	10	4
7/1/2000	7:01:55.58	6.8	34.22	139.13	10	8
7/2/2000	8:57:51.37	4.1	34.01	139.36	10	4
7/2/2000	20:03:34.8	5.7	34.08	139.23	10	5
7/8/2000	18:57:44.47	6.6	34.31	139.26	10	8
7/11/2000	18:23:51.02	5.1	34.22	138.95	10	7
7/12/2000	11:10:00.82	4.1	34.15	139.29	10	3
7/12/2000	7:49:10.79	4.3	34.13	139.18	10	6
7/12/2000	8:43:08.1	4.3	34.23	139.28	10	7
7/15/2000	1:05:35.43	4.4	34.15	138.95	10	3
7/15/2000	1:30:30.5	6.1	34.32	139.26	10	6
7/18/2000	12:22:10.95	4.7	34.06	139.19	10	4
7/19/2000	11:00:39.44	5.0	34.24	139.13	10	5
7/19/2000	17:32:19.94	5.2	34.17	139.13	10	7
7/20/2000	18:39:18.82	6.2	36.51	140.98	47	3
7/22/2000	15:24:35.76	4.4	34.23	139.20	10	6
7/23/2000	3:15:08.34	5.3	34.23	139.25	10	6
7/23/2000	21:52:44.06	5.6	34.13	139.12	10	5
7/27/2000	2:15:16.24	4.7	34.18	139.32	10	6
7/27/2000	1:49:53.33	5.6	34.21	139.37	10	6
8/3/2000	13:18:09	5.5	34.17	139.14	10	8
8/14/2000	18:54:59.12	3.8	36.16	139.85	92	4
8/18/2000	1:52:20.87	5.7	34.13	139.18	10	4
8/23/2000	14:57:11.63	5.4	34.07	139.45	10	4
10/6/2000	4:30:19.15	7.4	35.46	133.13	10	2
10/8/2000	4:17:55.12	5.4	35.15	133.04	10	2
10/15/2000	23:40:21.5	3.8	35.39	140.32	66	4
11/13/2000	19:13:22.8	4.0	35.67	140.20	71	7
11/13/2000	15:57:21.61	6.0	42.49	144.76	33	3
3/24/2001	6:27:53.58	6.8	34.08	132.53	50	6
12/2/2001	13:01:53.67	6.5	39.40	141.09	123	4
10/14/2002	14:12:43.75	6.1	41.17	142.25	61	3
11/3/2002	3:37:42.07	6.4	38.89	141.98	39	3

$$\frac{\int_0^{t_0} \dot{x}^2(t) dt}{\int_0^{t_0} x^2(t) dt}$$

is the spectrally weighted average of angular frequency squared with the weight equal to the modulus squared of the velocity spectrum (Wu and Kanamori, 2005). In our implementation, τ is calculated recursively and $t = 0$ is an arbitrary starting time. The introduction of α in equation (1) has the effect of applying a high-pass filter to the time series. With the proper choice of α , the contribution to τ given by equation (5) comes from x^2 near t_0 , while still providing a measure of the spectrally weighted average of angular frequency squared with the weight equal to the modulus squared of the velocity spectrum.

What is important to the present study is that this empirical observation provides a parameter that scales with the magnitude of earthquakes. Figure 2 shows an example vertical velocity waveform from each region and the T^p time series derived from them. In the Pacific Northwest the noise is longer period than the P wave and T^p drops at the time of the P arrival (Fig. 2a), whereas the reverse is true for the Japan example (Fig. 2b).

For the purpose of magnitude determination we only monitor T_i^p for the first 5 sec after the P -wave trigger and

record the maximum predominant period observed, T_{\max}^p . At lower magnitudes (M 3.5–5.0) T_{\max}^p is usually observed during the first 3 sec, whereas larger events typically require 4 sec of data, and occasionally 5 sec. We do not use T_i^p immediately after the trigger because we must allow for the transient (due to smoothing terms in equations 2 and 3) between T_i^p of the background noise before the trigger and T_i^p of the P wave. The nature and duration of the transient depends on the change in frequency content (which varies from region to region), and whether the arrival is emergent or impulsive. Also, T^p can oscillate about a mean value for the first 1 or 2 sec as shown in Figure 2b. This is an artifact of the manner in which T^p is calculated. When using data from the Pacific Northwest we do not use 0.5 sec of the T^p trace after the trigger to avoid these transients (the same 0.5 “blackout” window was found to be optimal in southern California [Allen and Kanamori, 2003]). However, analysis of the Japan dataset indicates that a 2-sec blackout window before measuring T_{\max}^p improves the magnitude-period scaling relation significantly. Figure 3 shows the time-frequency transform of the velocity waveform shown in Figure 2b. T_{\max}^p is observed at 25.75 sec and is indicated in time-frequency space as the black dot in Figure 3. The plot shows how T_{\max}^p represents a spectral average for the waveform.

The accuracy and sensitivity of the magnitude estimate can be improved by selecting the optimal frequency band at

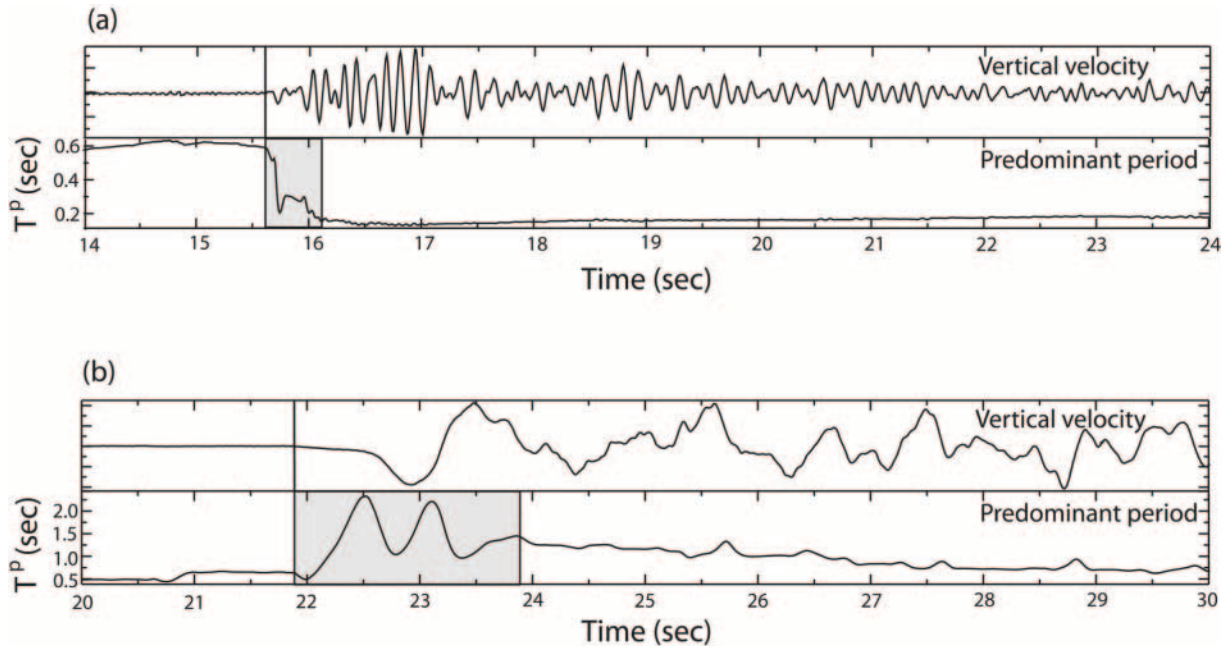


Figure 2. Seismograms and predominant period plots from a magnitude 4.5 earthquake in the Pacific Northwest (a) and a magnitude 5.7 earthquake in Japan (b). Because of transients between the frequency content of background noise and the P wave we do not use the predominant period trace immediately after the trigger. For the Pacific Northwest dataset we do not use the first 0.5 sec, whereas we find the best magnitude-period scaling relation when we do not use the first 2 sec in Japan. This is due to large oscillations in the predominant period after the trigger, as shown in (b). The maximum predominant period within 5 sec is then used in our scaling relations.

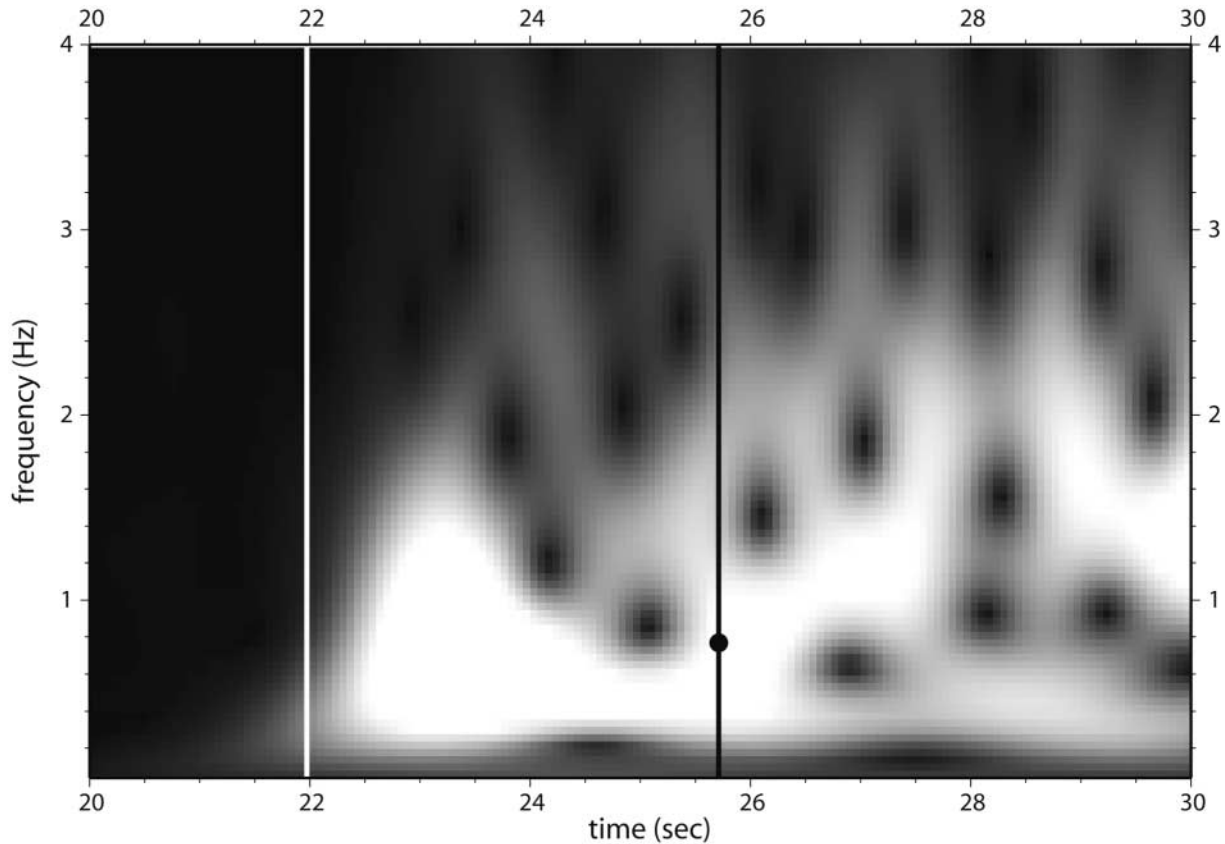


Figure 3. Time-frequency transform showing the amplitude spectra for the velocity waveform shown in Figure 2b. White regions show high amplitude. The white line shows the time of the trigger and the black dot indicates the location of the T_{\max}^p observation in time-frequency space.

which T_{\max}^p is observed. Applying a low-pass filter to the waveforms reduces the high-frequency noise and improves the signal-to-noise ratio. Using different low-pass filters for low- and high-magnitude events produced the best estimates of magnitude in the California study: a 10-Hz low-pass filter improved the magnitude-period scaling relation for small magnitude events ($M < 5$), and a 3-Hz low-pass filter was found to be optimal for events with $M > 4.5$ (Allen and Kanamori, 2003). Both the Pacific Northwest and Japan datasets were evaluated by using 10-Hz and 3-Hz low-pass filters to compare with previous results. The datasets were also evaluated with a range of low-pass filters to determine which filters maximize the sensitivity of magnitude-period relations and reduce the scatter of the predominant period measurements.

Magnitude-Period Relations

Magnitude-period relations for the Pacific Northwest and Japan, having low-pass filtered the data at 10 Hz and 3 Hz, are shown in Figure 4. All panels in Figure 4 show T_{\max}^p observation from individual stations as gray dots and the average T_{\max}^p observation for each event as a black dot.

The best-fit linear relation between magnitude and the event-averaged predominant period is shown (solid line) along with the best fit previously found for California (dashed). Figure 4a shows that lower-magnitude events ($M < 5.0$) do not show significant differences in T_{\max}^p when passed through a 10-Hz low-pass filter. In fact, there is little sensitivity of T_{\max}^p to magnitude regardless of the filter for low-magnitude events in the Pacific Northwest. Figure 4b shows there is a marked increase in T_{\max}^p with increasing magnitude for events ranging from 5.0 to 6.8 when the waveforms are passed through a 3-Hz low-pass filter, although this observation is based on only a few earthquakes because the limited data available for large-magnitude events in the region. However, the best-fit scaling relation between T_{\max}^p and magnitude is similar to that found in southern California.

The Japanese dataset shows scaling relations when the data are low-pass filtered at both 10 and 3 Hz. Figure 4c shows the low-magnitude (M 3.8–5.0) scaling relation having low-passed the waveforms at 10 Hz and ignoring the first 2 sec of the P -wave arrival. Figure 4d shows the high-magnitude (M 5.0–7.4) scaling relation once the waveforms are low-pass filtered at 3 Hz, also ignoring the first 2 sec of the signal prior to measuring T_{\max}^p . The relations between

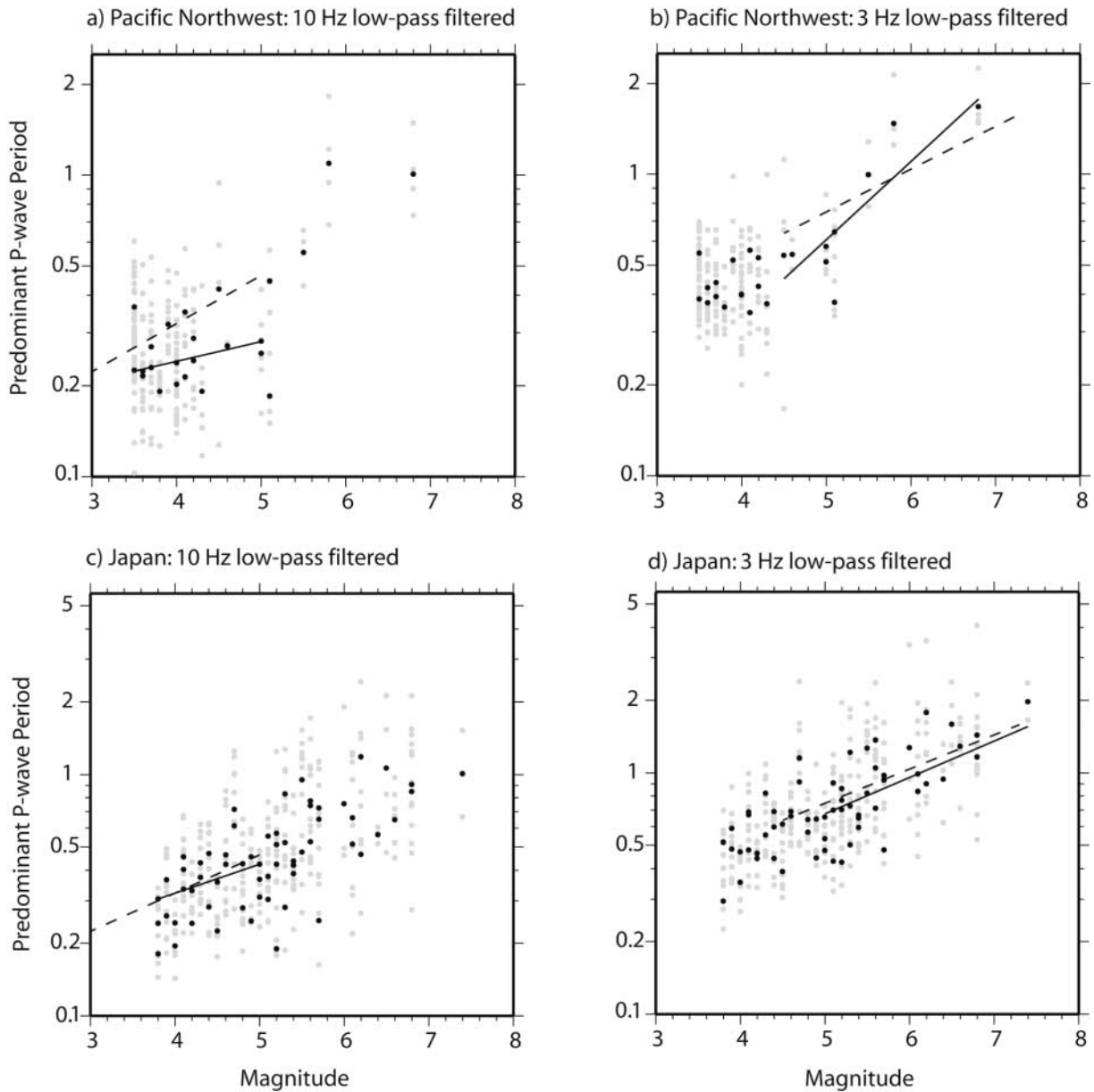


Figure 4. Scaling relations between earthquake magnitude and the predominant period of the P wave for earthquakes in the Pacific Northwest (a and b) and Japan (c and d) having low-passed the velocity waveforms at 10 Hz and 3 Hz prior to calculating the predominant period. Earthquakes from the Pacific Northwest show the best scaling relation when 1 sec of the P wave is used for the low-magnitude events (a) and when 4 sec of data is used for the high-magnitude events (b). Earthquakes in Japan show the best relation when 3 sec of the P wave is used for the low-magnitude events (c) and when 4 sec of data is used for the high-magnitude events (d). Gray dots show the predominant period measurements of individual stations; black dots show the average predominant period for each event. Black lines show the best-fit scaling relation for the event averages. For comparison, the best-fit scaling relations for the southern California dataset (Allen and Kanamori, 2003) are shown with a dashed black line.

T_{\max}^p and magnitude are almost identical with the results of the southern California study, as shown by the near overlap of the dashed best-fit line from the southern California relation and the solid best-fit line for Japan. The similarity of the results is important given the differences in geologic set-

tings, the increase in the number of high-magnitude events in the Japan dataset, and the fact that the previous study used waveforms recorded within 100 km of the epicenter, a distance that was increased to 150 km for this study.

To explore the sensitivity of the magnitude-period re-

lations with respect to filters used, we apply a variety of low-pass filters to the Japanese dataset and determine the gradients and the average absolute deviation of the best-fit lines. The filter that produced the greatest sensitivity of T_{\max}^p to magnitude with least scatter was selected as being the most favorable. The optimal magnitude-period relations are attained when low-magnitude events (M 3.8–5.0) are low-pass filtered at 5 Hz, and when a 1-Hz low-pass filter is applied to the waveforms of higher-magnitude events (Fig. 5). The best-fit magnitude-period scaling relations are:

$$m_l = 6.1 \log(T_{\max}^p) + 6.7 \quad (6)$$

$$m_h = 4.7 \log(T_{\max}^p) + 4.8 \quad (7)$$

where m_l is the estimated magnitude having low-passed the data at 5 Hz and is appropriate for low-magnitude ($M < 5$) events, and m_h is the estimated magnitude having low-passed the data at 1 Hz and is appropriate for high-magnitude events. These relations were obtained by minimizing the absolute deviation of the event-averaged T_{\max}^p observations, i.e., minimizing the l^1 norm. The goodness of fit is expressed in terms of the average absolute deviation of the observations from the best-fit line. $\log(T_{\max}^p)$ is the independent variable and the average deviation of the $\log(T_{\max}^p)$ values are translated into deviations in magnitude using the gradient of the best-fit line. These average absolute deviations are 0.55 magnitude units for m_l and 0.36 for m_h . Note that these best-fit relations use the event-averaged values of T_{\max}^p and

the average deviations are for event averages. The average deviations of individual station observations are larger, 0.84 magnitude units for m_l and 0.73 for m_h . What this means for the accuracy of magnitude estimates of an early warning system is discussed in the next section.

The magnitude-period scaling relations (equations 6 and 7) are derived from the average T_{\max}^p for each event. As shown in Figures 4 and 5 the variability in individual station observations of T_{\max}^p (gray dots) is considerably greater than event-averaged values (black dots). Inspection of magnitude-period plots created for individual stations in Japan shows variability in the scaling relations (Fig. 6). Although some stations exhibit T_{\max}^p measurements that increase steadily with magnitude (e.g., Fig. 6a), others exhibit no apparent relation (Fig. 6b). These apparent differences in the quality of magnitude information available from different stations have also been observed in California (Lockman and Allen, 2005).

Magnitude Estimate Errors

To test the potential accuracy of magnitude estimates derived from T_{\max}^p observations in Japan, we estimate the magnitude of each event using best-fitting scaling relations determined without the use of data from the event being considered. For each event in turn, new scaling relations between T_{\max}^p and magnitude are determined with the same approach as for equations (6) and (7) but excluding data

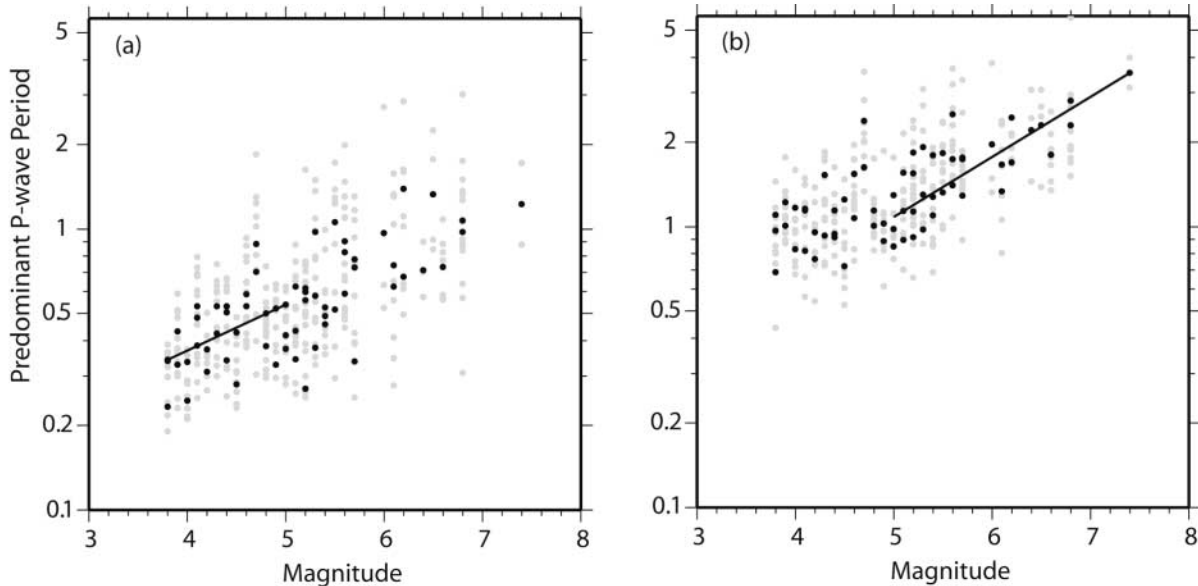


Figure 5. Optimal magnitude-period relationships for the Japan dataset: (a) the low-magnitude relationship using three seconds of waveform data low-pass filtered at 5.0 Hz; (b) the high-magnitude relationship after waveforms are low-pass filtered at 1.0 Hz and 4 sec of data are used. Gray dots are the maximum predominant period observations at individual stations and the black dots are event averages. The lines represent best-fit scaling relationships for this dataset.

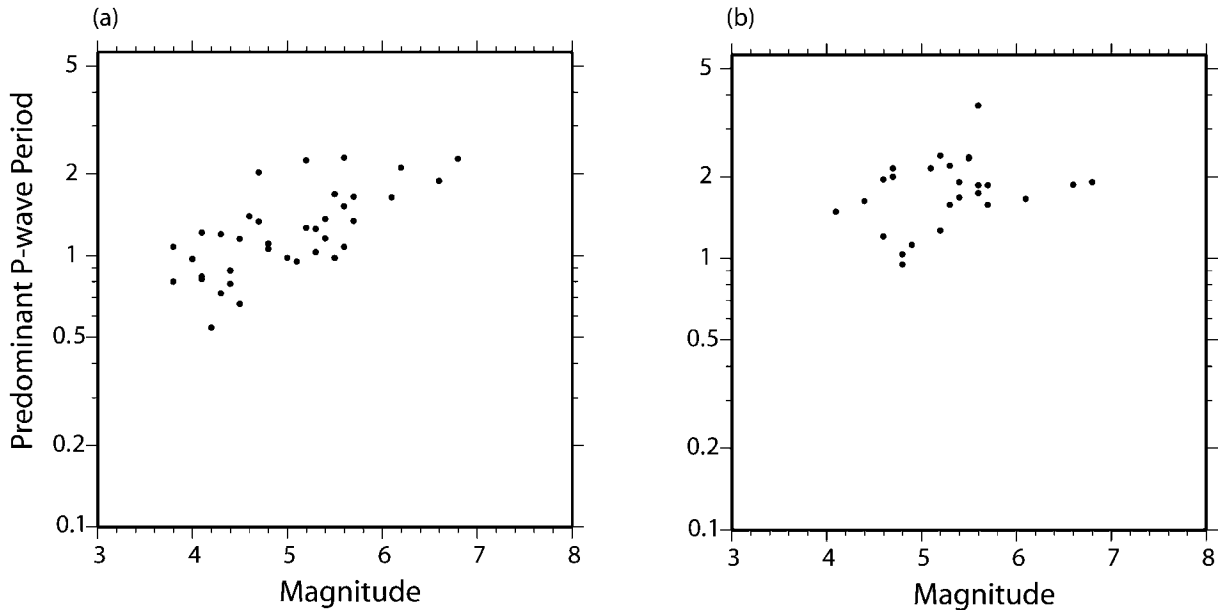


Figure 6. The maximum predominant period is plotted against the event magnitude for two individual stations in Japan. Although (a) shows scaling between magnitude and predominant period for station JIZ, (b) indicates there is no such scaling relation observed at station SMZ. Both show the predominant period measured using 4 sec of data after the waveforms are passed through a 1.0-Hz low-pass filter. Both stations were used as part of the complete Japanese dataset included in Figures 4 and 5, and the magnitude estimate analysis results shown in Figure 7.

from the current event. The waveforms for the current event are low-pass filtered at 5 Hz, and the T_{\max}^p is calculated using 3 sec of data, and also low-pass filtered at 1 Hz and the T_{\max}^p is calculated using 4 sec of data. An initial magnitude estimate is calculated assuming a low-magnitude event, i.e., using the T_{\max}^p value from the 5-Hz-filtered waveform and the scaling relation for low-magnitude events (equivalent to equation 6). If this magnitude estimate is greater than 5.0, it is replaced with the magnitude estimate derived from the T_{\max}^p value from the waveform filtered at 1 Hz and the high-magnitude relation (equivalent to equation 7). Event magnitude estimates are determined using just the closest station to the epicenter, then the closest two stations and so on up to a maximum of eight stations. Figure 7 shows the average absolute error in the event-magnitude estimates for all earthquakes versus the number of stations providing a T_{\max}^p observation. The magnitude estimate becomes more accurate as additional stations are used, with the average magnitude error decreasing from 0.75 magnitude units with one station, to 0.66, 0.57, and 0.49 magnitude units with two, three, and four stations respectively. The dataset from Japan shows no improvement in the accuracy of the magnitude estimate when more than four stations are used. This is similar to the observation of Allen and Kanamori (2003) for southern California. They found that the average error using the first station to trigger was 0.70 and reduced to 0.45 using the closest four stations.

Application to Early Warning

Because cities in seismically hazardous regions are expected to continue experiencing rapid population growth and urbanization in the future (Bilham, 2004), there is a need for increased disaster prevention to protect infrastructure, industry, and populations. Accurate short-term forecasts of the time, location, and magnitude of an earthquake have proved elusive, but EWSs provide an alternative approach to short-term mitigation and have many applications that can lessen the damaging effects of earthquakes.

Three geologically diverse regions, Japan, the Pacific Northwest, and southern California, suggest that the T^p of the P wave can be used to estimate earthquake magnitude before the S -wave arrival, indicating that P -wave detection can be used to issue a warning before significant ground shaking begins. Because the P wave is the first energy pulse to arrive during an earthquake, this is the quickest method of estimating event magnitude for the purpose of early warning. Warning times increase with epicentral distance, but P -wave detection can potentially provide a warning to system users in the epicentral region. Our results also indicate that a reasonably accurate magnitude estimate is obtained using four seismic stations, an observation supported by a similar analysis of the southern California dataset. Thus, a network of four seismic stations may be the minimum required to provide a low-cost earthquake mitigation measure where building codes are nonexistent or ineffective.

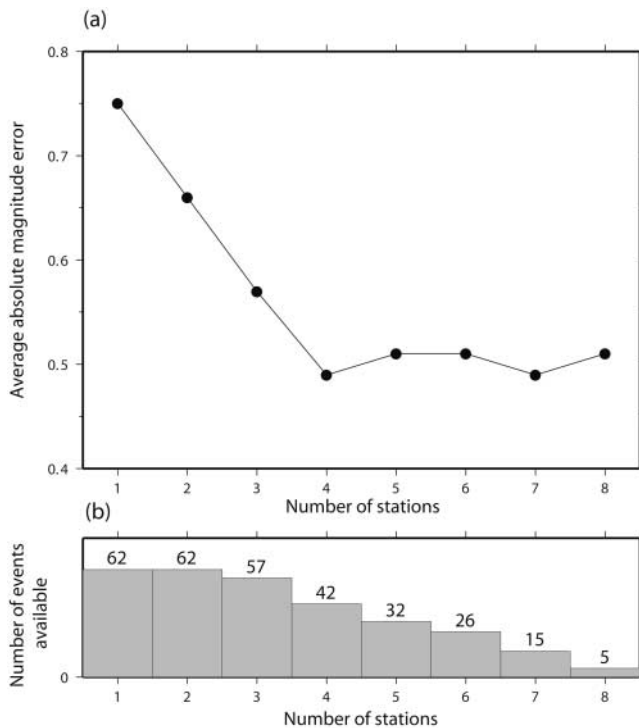


Figure 7. (a) Average absolute magnitude error for all events calculated as a function of the number of stations providing a predominant period estimate. When using one station we only use the closest station to the epicenter. The average for two stations uses the closest two stations etc. (b) The number of events available with 1, 2, 3, etc. waveforms within 150 km from which the average magnitude error in (a) is calculated. The plot shows the significant improvement in the magnitude estimate as observations become available from the second, third, fourth station. In this Japan dataset, there is little observed improvement using more than four stations.

Because of the potentially high economic costs and resulting social disruption of a false positive, users of early warning technology must apply the system in a manner that complements other earthquake mitigation measures and in such a way that losses due to false alarms are at an acceptable level. Therefore, users of the warning system must determine hazard and certainty thresholds that are appropriate for their needs. Proper application requires consideration of the cost of a false alarm with respect to the potential safety gains of individual users. Systems may also operate “silently” to automatically protect infrastructure without human intervention to maintain useful warning times (Allen, 2006). Examples of existing applications in Mexico, Japan, Taiwan, and Turkey include schools, hospitals, homes, private industry, rail, and utility companies. In the future infrastructure may be able to make use of the warning information to better protect people and property. One example being explored in Japan is the use of active response systems in buildings (Housner *et al.*, 1997).

Another important application of EWSs is to protect di-

saster relief workers from falling debris while performing rescue and recovery operations in the wake of a damaging earthquake. Structures damaged during an earthquake are in a severely weakened state and susceptible to additional failure or collapse during aftershocks, thereby posing a significant threat to rescue workers searching for survivors and removing debris. This is a prime situation for EWSs because the level of risk is heightened, there is increased seismicity in the form of aftershocks, the likely source area is known, and the tolerance for false alarms is higher. In these situations a temporary network can be deployed in the epicentral region to communicate aftershock information to workers in the damage zone. A portable front detection EWS was used after the M 7.1 Loma Prieta earthquake to reduce the risk to relief crews in the San Francisco Bay Area (Bakun *et al.*, 1994).

Summary

1. Results from the Pacific Northwest and Japan show a scaling relation between earthquake magnitude and predominant period of the first few seconds of the P wave. The relations are similar to those previously observed in southern California (Allen and Kanamori, 2003; Allen, 2004; Lockman and Allen, 2005). The similarity of the scaling relations derived from datasets from different regions shows that the magnitude-period relations are not sensitive to the variable attenuation characteristics of the different geologic environments or faulting style. Furthermore, the results presented here suggest that useful predominant period observations can be made at stations up to 150 km from the source.
2. The sensitivity of magnitude-period relations can be optimized using different frequency bands of the waveform. Sensitivity to large-magnitude events (i.e., $M > 4.5$) is maximized by low-pass filtering with a lower corner frequency than for small-magnitude events. Slightly different corner frequencies of the applied low-pass filters are found to be optimal for different regions. Earthquakes in southern California and the Pacific Northwest show maximum sensitivity of T_{\max}^p to magnitude when waveforms are low-pass filtered at 10 Hz for $M < 5.0$, and 3 Hz for $M > 4.5$, whereas the Japan dataset shows maximum sensitivity when low-pass filtered at 5 Hz for $M < 5.0$ and 1 Hz for $M > 5.0$.
3. The accuracy of the magnitude estimate increases as the number of stations providing predominant period observations increases. Our results show that for the Japan dataset the error in the magnitude estimations decreases substantially once four stations provide predominant period estimates compared with a single-station estimate. The average error of the magnitude estimate is 0.75 using one station and drops steadily to 0.49 once four stations are available.
4. The use of the P -wave arrival to assess the hazard posed by an earthquake maximizes the warning time available

and could provide a warning in the epicentral region. Datasets from Japan and southern California show that magnitude estimates with average errors of less than half a magnitude unit are obtained with four seismic stations. This makes it possible to apply early warning mitigation strategies without the need for dense seismic networks at relatively low cost.

Acknowledgments

We thank Hiroo Kanamori, Yih-Min Wu, and Yutaka Nakamura for helpful discussions about this work. Gerardo Suárez, J. Pujol, and an anonymous reviewer provided helpful comments during the preparation of this manuscript. Data from the Pacific Northwest Seismic Network was provided by the Data Management Center of the Incorporated Research Institutions for Seismology, data from Japan came from F-net operated by the National Research Institute for Earth Science and Disaster Prevention. Funding for this study was provided by U.S. Geological Survey/National Earthquake Hazards Reduction Program awards 03HQGR0043 and 05HQGR0074, the Graduate School of the University of Wisconsin-Madison and BP. The figures were produced with SAC and GMT (Wessel and Smith, 1995).

References

- Allen, R. M. (2004). Rapid magnitude determination for earthquake early warning, in *The Many Facets of Seismic Risk*, M. Pecce, G. Manfredi, and A. Zollo (Editors), Università degli Studi di Napoli "Federico II", Napoli, 15–24.
- Allen, R. M. (2006). Probabilistic warning times for earthquake ground shaking in the San Francisco Bay Area, *Seism. Res. Lett.* **77**, 371–376.
- Allen, R. M., and H. Kanamori (2003). The potential for earthquake early warning in southern California, *Science* **300**, 786–789.
- Bakun, W. H., F. G. Fischer, E. G. Jensen, and J. Vanschaack (1994). Early warning system for aftershocks, *Bull. Seism. Soc. Am.* **84**, 359–365.
- Bilham, R. (2004). Urban earthquake fatalities: a safer world, or worse to come? *Seism. Res. Lett.* **75**, 706–712.
- Boese, M., M. Erdik, and F. Wenzel (2004). Real-time prediction of ground motion from P-wave records (abstract), *EOS Trans. AGU* **85** (Fall Meet. Suppl.), S21A.0251.
- Erdik, M. O., Y. Fahjan, O. Ozel, H. Alcik, M. Aydin, and M. Gul (2003). Istanbul Earthquake Early Warning and Rapid Response System (abstract), *EOS Trans. AGU* **84** (Fall Meet. Suppl.), S42B.0153.
- Espinosa-Aranda, J. A., A. Jimenez, G. Ibarrola, F. Alcantar, A. Aguilar, M. Inostroza, and S. Maldonado (1995). Mexico City seismic alert system, *Seism. Res. Lett.* **66**, 42–53.
- Frankel, A., C. Mueller, T. Barnhard, D. Perkins, E. V. Leyendecker, N. Dickman, S. Hanson, and M. Hopper (1996). National seismic hazard maps, series, *U.S. Geol. Surv. Open-File Rept.* 96-532.
- Grecksch, G., and H. J. Kumpel (1997). Statistical analysis of strong-motion accelerograms and its application to earthquake early-warning systems, *Geophys. J. Int.* **129**, 113–123.
- Horiuchi, S., H. Negishi, K. Abe, A. Kamimura, and Y. Fujinawa (2005). An automatic processing system for broadcasting earthquake alarms, *Bull. Seism. Soc. Am.* **95**, 708–718.
- Housner, G. W., L. A. Bergman, T. K. Caughey, A. G. Chassiakos, R. O. Claus, S. F. Masri, R. E. Skelton, T. T. Soong, B. F. Spencer, and J. T. P. Yao (1997). Structural control: past, present, and future, *J. Eng. Mech. ASCE* **123**, 897–971.
- Kamigaichi, O. (2004). JMA earthquake early warning, *J. Jpn. Assoc. Earthquake Eng.* **4**, 1–4.
- Lockman, A., and R. M. Allen (2005). Single station earthquake characterization for early warning, *Bull. Seism. Soc. Am.* **95**, 2029–2039.
- Ludwin, R. S., A. I. Qamar, S. D. Malone, C. Jonientz-Trisler, R. S. Crosson, R. Benson, and S. Moran (1994). Earthquake hypocenters in Washington and northern Oregon, 1987–1989 and the Washington Regional Seismograph Network, Operations and Data Processing, Series, Washington State Department of Natural Resources, Information Circular 89.
- Nakamura, Y. (1988). On the urgent earthquake detection and alarm system (UrEDAS), in *Proc. Ninth World Conference on Earthquake Engineering VII*, 673–678.
- Nakamura, Y. (2004). UrEDAS, Urgent earthquake detection and alarm system, now and future, presented at *13th World Conf. Earthquake Eng.*, August 2004, paper no. 908.
- Nakamura, Y., and B. E. Tucker (1988). Earthquake warning system for Japan railways' bullet train: implications for disaster prevention in California, *Earthquakes Volcanoes* **20**, 140–155.
- Odaka, T., K. Ashiya, S. Tsukada, S. Sato, K. Ohtake, and D. Nozaka (2003). A new method of quickly estimating epicentral distance and magnitude from a single seismic record, *Bull. Seism. Soc. Am.* **93**, 526–532.
- Okada, Y., K. Kasahara, S. Hori, K. Obara, S. Sekiguchi, H. Fujiwara, and A. Yamamoto (2004). Recent progress of seismic observation networks in Japan—Hi-net, F-net, K-NET, KiK-net, *Earth, Planets and Space* **56**, xv–xxviii.
- Olson, E., and R. M. Allen (2005). The deterministic nature of earthquake rupture, *Nature* **438**, 212–215.
- Olson, E. L., and R. M. Allen (2006). Is earthquake rupture deterministic? (Reply), *Nature* **442**, E6.
- Rydelek, P., and S. Horiuchi (2006). Is earthquake rupture deterministic? *Nature* **442**, E5–E6.
- Simons, F. J., B. Dando, and R. M. Allen (2006). Automatic detection and rapid determination of earthquake magnitude by wavelet multiscale analysis of the primary arrival, *Earth Planet. Sci. Lett.* **250**, 214–223.
- Wald, D. J., V. Quitoriano, T. H. Heaton, H. Kanamori, C. W. Scrivner, and C. B. Worden (1999). TriNet "ShakeMaps": rapid generation of peak ground motion and intensity maps for earthquakes in southern California, *Earthquake Spectra* **15**, 537–555.
- Wessel, P., and W. H. F. Smith (1995). New version of the Generic Mapping Tools released, *EOS Trans. AGU* **76**, 329.
- Wolfe, C. J. (2006). On the properties of predominant period estimators for earthquake early warning, *Bull. Seism. Soc. Am.* **96**, 1961–1965.
- Wu, Y.-M., and H. Kanamori (2005). Experiment on an onsite early warning method for the Taiwan Early Warning System, *Bull. Seism. Soc. Am.* **95**, 347–353.
- Wu, Y. M., and T. L. Teng (2002). A virtual subnetwork approach to earthquake early warning, *Bull. Seism. Soc. Am.* **92**, 2008–2018.
- Wu, Y. M., T. C. Shin, and Y. B. Tsai (1998). Quick and reliable determination of magnitude for seismic early warning, *Bull. Seism. Soc. Am.* **88**, 1254–1259.

Department of Geology and Geophysics
University of Wisconsin
Madison, Wisconsin 53706
(A.B.L.)

Department of Earth and Planetary Sciences
University of California
Berkeley, California 94720
rallen@berkeley.edu
(R.M.A.)